Journal of Power Sources 195 (2010) 3091–3096

Contents lists available at ScienceDirect

Journal of Power Sources

journal homepage: www.elsevier.com/locate/jpowsour

The effect of overpotential on performance degradation of the solid oxide fuel cell Ni/YSZ anode during exposure to syngas with phosphine contaminant

Oktay Demircan[a,*], Wei Zhang[a], Chunchuan Xu[b], John Zondlo[b], Harry O. Finklea[a,c]

[a] C. Eugene Bennett Department of Chemistry, West Virginia University, 217 Clark Hall Prospect Street, Morgantown, WV 26506, USA
[b] Department of Chemical Engineering, West Virginia University, Morgantown, WV 26506, USA
[c] National Energy Technology Laboratory-Institute for Advanced Energy Studies, US Dept. of Energy, Morgantown, WV 26505, USA

ARTICLE INFO

Article history:
Received 13 October 2009
Received in revised form
17 November 2009
Accepted 25 November 2009
Available online 2 December 2009

Keywords:
SOFC
Syngas
Phosphine
Degradation
Overpotential
Polarization resistance and ohmic resistance

ABSTRACT

Phosphine (PH_3) as a contaminant in coal syngas has been shown to cause permanent degradation on solid oxide fuel cell (SOFC) anode performance. Previous studies on the performance degradation have been performed at constant current or constant voltage over the entire experiment. In this work, the effect of overpotential (difference between the open circuit voltage and the applied voltage) on rates of degradation of SOFC performance is examined. A commercial SOFC from MSRI is exposed in sequence to first hydrogen, then coal syngas and then coal syngas with 10 ppm PH_3. The rates of cell power density loss rates are monitored for three overpotentials (0.1, 0.2 and 0.3 V). There is no apparent correlation between the degradation rates and overpotential values. Post-mortem studies including SEM, XRD and XPS confirm the migration of nickel to the anode surface and the formation of a nickel phosphide phase.
Published by Elsevier B.V.

1. Introduction

Coal syngas has the great potential to be one of the logistic fuels for solid oxide fuel cells in the near future. The effect of syngas contaminants on the Ni/YSZ anode has been a popular research subject [1]. Volatile phosphorus species in syngas, particularly phosphine (PH_3), are known to cause irreversible and immediate degradation of the performance of the Ni/YSZ anode [2–7]. The degradation of Ni/YSZ anode performance due to the presence of PH_3 at ppm levels could be the result of two different mechanisms: (i) the loss of Ni (loss of TPB length) in the active layer of the anode via nickel migration out of the anode active layer due to facile reactions between Ni and P and (ii) the production of Ni–P compounds resulting in a decrease in the number of active Ni sites in catalytic anode layer. The active sites of Ni catalyze both fuel oxidation and the water gas shift reaction. Kishimoto et al. [8] have examined the chemical stability of the Ni/YSZ anode with respect to the gaseous impurities containing phosphorus compounds. Their Ellingham diagrams for the P–O–H and the Ni–P–OH systems demonstrate that Ni phosphides can easily form even at very low PH_3 concentrations.

Previous work on PH_3 contamination has used a constant current density or a constant voltage as the operating condition [4,5]. Based on anticipated use in power generation, the standard operating condition of SOFCs is usually around 0.7–0.8 V for the cell voltage. Defining overpotential as the difference between the open circuit voltage and applied voltage, the operation conditions are around 0.2–0.4 V overpotential depending on the fuel mixture and assuming air is the cathode feed. The correlation of overpotential and degradation rates during exposure to PH_3 in ppm level could supply valuable information about the performance degradation. Liu and co-workers [9,10] have studied the effect of overpotential on sulfur poisoning rate and recovery in sulfur-free fuel. Their experimental results show that an increase in cell overpotential (increase in current density) coincides with a smaller relative internal resistance increase during sulfur poisoning. This effect could be explained by the acceleration of sulfur oxidation by oxide ions as an increased current density raises the flux of oxide ions to the anode.

In this study, a long term SOFC test on a single commercial SOFC is reported. The test includes performance under H_2 and then a syngas fuel mixture, the latter mixture without and then with 10 ppm phosphine as an impurity. The effects of different overpotential levels on the degradation rates were monitored. Specifically, the cell was held at a constant overpotential of 0.1, 0.2 and 0.3 V for at least 24 h at each overpotential. The 24 h was long enough to measure rates of degradation and short enough to avoid major

* Corresponding author. Tel.: +1 304 293 3435x6440; fax: +1 304 293 4904.
E-mail addresses: Oktay.Demircan@mail.wvu.edu, okdemircan@mail.wvu.edu (O. Demircan).

0378-7753/$ – see front matter. Published by Elsevier B.V.
doi:10.1016/j.jpowsour.2009.11.114

changes in the cell performance. The sequence of overpotentials was repeated to check the reproducibility of the degradation. This strategy avoids complications due to lack of reproducibility of performance from one SOFC to the next. The test ended with operation on phosphine-free fuel to see if performance was recovered. Extensive post-mortem analysis techniques were employed to determine the chemical and physical nature of the Ni/YSZ anode after the prolonged exposure to phosphine with current flow. The main result of this study is that the degradation rate is not correlated with the overpotential.

2. Experimental methods

An anode-supported commercial MSRI cell (25 mm in diameter; ~0.8 mm 48% porous Ni/YSZ anode support layer; ~40 μm 23% porous Ni/YSZ active anode layer; ~10 μm dense YSZ electrolyte layer; ~40 μm 26% porous LSM/YSZ active cathode layer with 2 cm^2 area; ~40 μm 45% porous LSM/YSZ cathode layer with 2 cm^2 area) was mounted as shown in Fig. 1. The two Au leads on the anode surface and the Au gauze on the cathode surface appear in Fig. 1a and b, respectively. Two 4 mm × 4 mm Au electrodes were placed on the anode surface by using flattened gold wire and gold paste (BASF). One lead was used to carry current and the other to sense the anode potential. Most of the anode remained fully exposed to the fuel mixture. The gold mesh with gold paste on the periphery was used for the cathode current collector. Two gold wires, one for current-carrying and one for potential-sensing, were connected to the gold mesh.

The furnace and gas handling system details have been described in previous studies [4,5]. The furnace temperature was increased to 800 °C at the rate of 2 °C min^{-1}, while exposing the anode to a dry H_2 (30 sccm)–N_2 (200 sccm) gas mixture and the cathode to air (200 sccm). The cell was held at 800 °C for about 12 h to produce a fully reduced Ni/YSZ anode. The flow rate of H_2 was increased to 200 sccm with 3% water vapor provided by a humidifier and the flow rate of air to the cathode was increased to 300 sccm. The cell load was set at a constant current of 0.5 A cm^{-2} while monitoring the voltage for a day. At the end of the experiment, the SOFC temperature was then decreased to room temperature with the rate of 2.5 °C min^{-1} under 20 sccm (10%) H_2 with 180 sccm (90%) N_2.

A Solartron SI 1287 potentiostat was employed for all electrochemical measurements. A Solartron SI 1260 impedance/gain-phase analyzer with AC amplitude of 20 mV at frequencies ranging from 100 kHz to 0.1 Hz was used for electrochemical impedance spectroscopy (EIS). Cell polarization curves and impedance spectra were obtained on a daily basis. The daily tests included operation for 1 min at a constant current density of 0.5 A cm^{-2} for comparison to previous experiments.

The following sequence of fuel mixtures was applied to the cell: (i) 194 sccm (97%) H_2 with 6 sccm (3%) water vapor for 70 h; (ii) 60 sccm (30%) H_2 plus 88 sccm (44%) N_2 with 52 sccm (26%) water vapor to mimic syngas mixture without CO/CO_2 for 24 h; (iii) syngas (60 sscm (30%) H_2, 52 sccm (26%) H_2O, 46 sccm (23%) CO, and 42 sccm (21%) CO_2) for 170 h; (iv) the same syngas with 10 ppm PH_3 for 170 h, (v) the same syngas without PH_3 for 16 h, and (vi) 60 sccm (30%) H_2 plus 88 sccm (44%) N_2 with 52 sccm (26%) water vapor for 24 h. During the PH_3 exposure, three different overpotential values (0.1, 0.2, and 0.3 V) were used to evaluate the effects of overpotential on the degradation rates of the cell performance. The program of overpotentials was repeated to check the reproducibil-

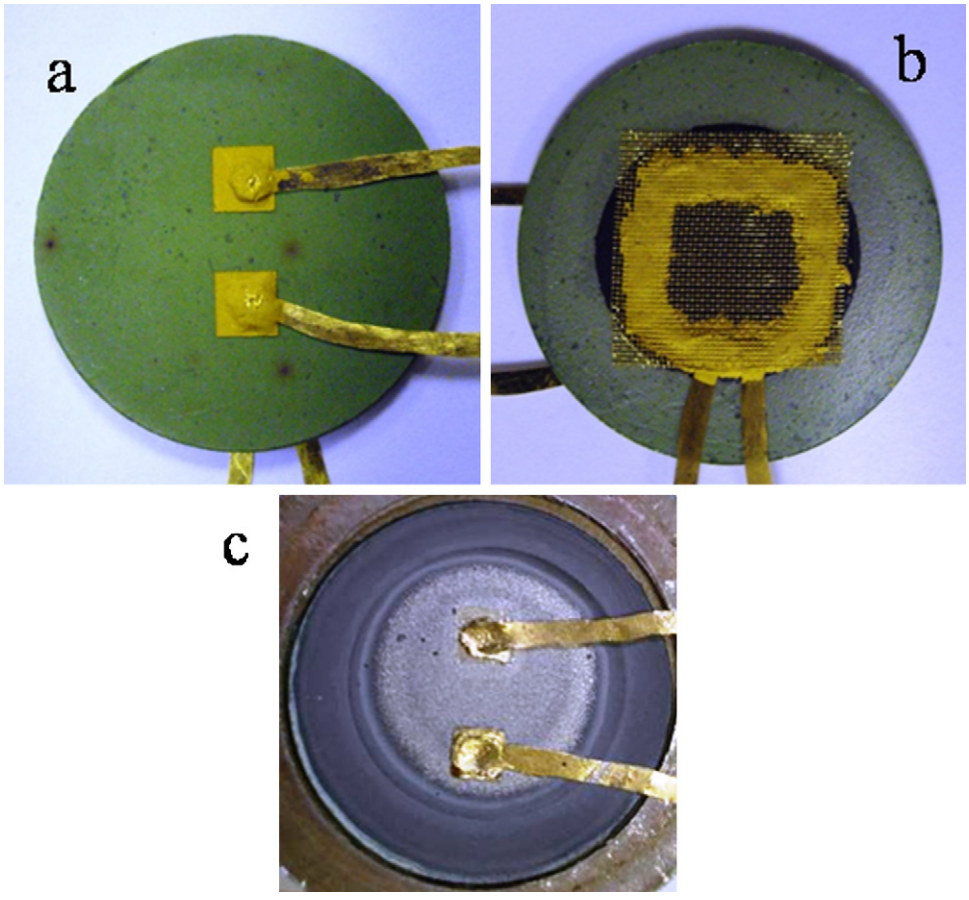

Fig. 1. Pictures of (a) the anode and (b) the cathode prior to mounting the SOFC. (c) The anode surface after operation in syngas with PH_3.

ity of the degradation rates. The overpotentials were corrected to the true overpotentials using the ohmic resistance from impedance measurements.

The surface and cross-section morphologies of the cell anode were studied with an SEM (JEOL-JSM 9490LV). XRD (Panalytical PM-3040 PRO), software (X'Pert Highscore Plus) and XPS (PHI 5000 VerasProbe XPS Microprobe) were employed to analyze the composition of the anode.

3. Results and discussion

Long term exposures are characterized by loss of current at a constant applied voltage, or loss of cell voltage at a constant applied current. For example, in the previous report [5], the cell voltage was monitored at a constant applied current. Performance density loss was expressed in terms of the average slope (e.g., 1.4 mV h^{-1} cm^{-2}). In this study, the cell was subjected to constant current or constant voltage, depending on the step. Consequently, degradation of performance during a step is described in terms of power loss (mW cm^{-2} h^{-1}). Degradation is also shown in terms of absolute parameters, the cell voltage at a constant current, and the total resistance measured by EIS at OCV and at 0.2 V overpotential (real impedance component at the lowest frequency). As noted in Section 2, these measurements were performed between the steps.

The initial performance of the cell was very good. In wet hydrogen, the peak power density was near 0.9 W cm^{-2} at 0.6 V, and in syngas, the peak power exceeded 0.6 W cm^{-2} at 0.5 V. The OCV in wet hydrogen was 1.068 V, somewhat lower than the Nernst value of 1.103 V for 97% hydrogen/3% water/air, and it remained at 0.944 V (Nernst value 0.948 V for $H_2/H_2O/O_2$) to within 1 mV during exposure to syngas without and with phosphine.

Corrected overpotentials are obtained by subtracting the *iR* drop (where *R* is the series resistance) from the applied overpotential. The series resistance measurements are shown in Fig. 2. The values are obtained from the high frequency intercept of the impedance with the real *Z*-axis in the Nyquist plot (see examples in Ref. [5]). This intercept is actually the upper bound for the series resistance because of the effects of a parallel combination of inductance and resistance (from the current-carrying leads) in series with the impedance of the cell. For example, equivalent circuit fitting of the data suggests that the actual series resistance is closer to 0.06 Ω cm^2

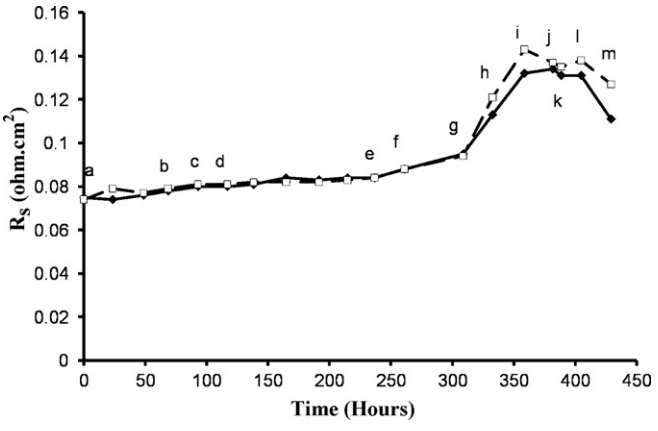

Fig. 2. Series resistances measured by EIS. Solid diamonds measured at OCV; open squares, measured at 0.2 V overpotential. Letters mark the changes in conditions. The series resistance is measured for the first condition listed in each step. (a) Start 97% H_2, 3% H_2. (b) End 97% H_2, 3% H_2O, start 30% H_2, 26% H_2O. (c) End 30% H_2, 26% H_2O, start pure syngas. (d) Continue pure syngas. (e) End pure syngas, start PH_3 exposure, apply 0.10 V. (f) End 0.10 V, apply 0.20 V. (g) End 0.20 V, apply 0.30 V. (h) End 0.30 V, apply 0.10. (i) End 0.10 V, apply 0.20 V. (j) End 0.20 V, apply 0.30 V. (k) End 0.30 V, begin syngas without PH_3. (l) End pure syngas, start 30% H_2, 26% H_2O. (m) End 30% H_2, 26% H_2O.

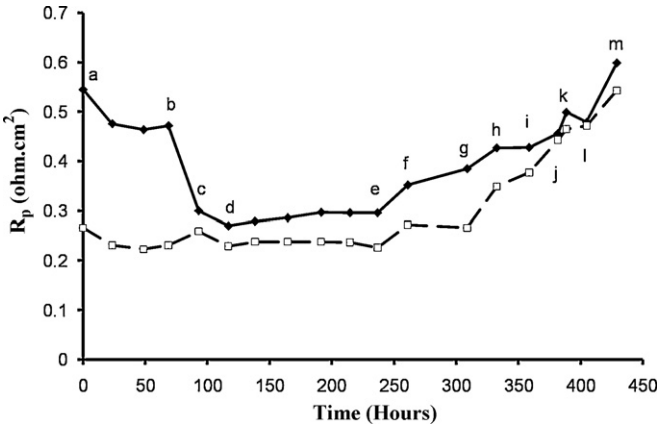

Fig. 3. Polarization resistances measured by EIS. Solid diamonds measured at OCV; open squares, measured at 0.2 V overpotential. Letters mark the changes in conditions. See the caption in Fig. 2.

when the intercept is near 0.08 Ω cm^2. However, the larger measured values are used in calculation of corrected overpotentials to avoid uncertainties caused by assuming values for the inductance and parallel resistance. Fig. 2 (points e–h) also shows that the series resistance rises significantly during the initial exposure to PH_3, remains nearly constant during subsequent exposures (points i–l), and then decreases during exposure to clean syngas (points l and m). To calculate the corrected overpotential, the average value of the series resistance in each step is used. During a step, the corrected overpotential is constant to the nearest 0.01 V. Applied overpotentials of 0.10, 0.20, and 0.30 V resulted in corrected overpotentials of 0.08, 0.16, and 0.23 V, respectively.

The corresponding polarization resistances are shown in Fig. 3. The drop in polarization resistance at OCV in the transition from wet hydrogen (97% H_2, 3% H_2O) to syngas (30% H_2, 26% H_2O, without and with CO and CO_2) is consistent with previous reports about the effect of higher water vapor concentrations [11,12] and its cause is attributed to an increase in the exchange current [13]. As with the series resistance, the values of the polarization resistance remain essentially constant until phosphine is introduced into the syngas mixture. Thereafter, the general trend is increasing polarization resistance even after the phosphine has been removed from the fuel. The latter observation may be due to desorption of residual PH_3 in the gas transfer lines.

The power density data at a constant current load of 0.5 A cm^{-2} is shown in Fig. 4. Power density is constant at 0.43 W cm^{-2} for three days of pure H_2 with 3% water. When the H_2 content is decreased to

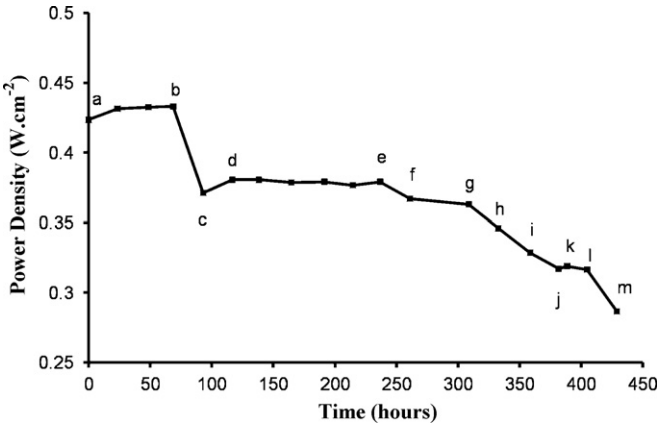

Fig. 4. Power density measured at a constant current of 0.5 A cm^{-2}. Letters mark the changes in conditions. See the caption in Fig. 2.

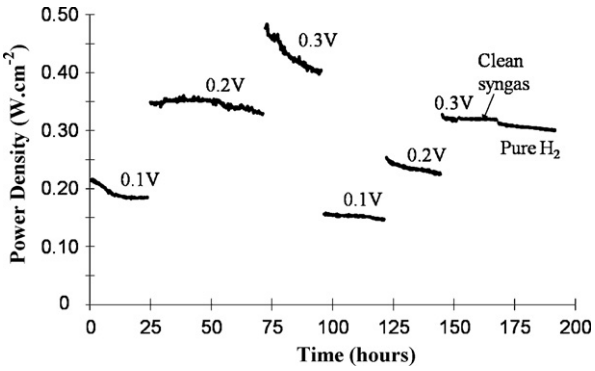

Fig. 5. Power degradation at different overpotentials during and after the exposure to PH_3.

30% and the water content is increased to 26% to mimic syngas mixture without CO and CO_2, power density decreases to 0.38 W cm^{-2}. Adding CO and CO_2, raises the power density slightly. During the course of syngas over a week, the value of power density under syngas is constant at 0.38 W cm^{-2}. Not surprisingly, in view of the resistance measurements in Figs. 2 and 3, introduction of 10 ppm PH_3 to the syngas fuel stream causes power density to decrease. This tendency of degradation in power density continues when PH_3 is taken out from fuel stream and also for 30% H_2 with 26% water.

Power vs. time plots during exposure to 10 ppm PH_3 and after exposure are shown in Fig. 5. For the first day of exposure to PH_3 at 0.1 V overpotential, the power curve is divided into two sections. Significant degradation occurs within the first 12 h, and then the rate of degradation decreases over the second 12 h. When the overpotential is increased to 0.2 V, no degradation is observed over the first 24 h, and then there is a noticeable degradation in the second 24 h. The highest degradation rate is observed at 0.3 V overpotential. The different overpotential tests were repeated to check the reproducibility of these degradation rates. Clearly, the degradation rates are not reproducible. The performance degradation occurs at all three overpotentials. No clear correlation exists between the overpotential and the degradation of power in the presence of PH_3 at 10 ppm.

The average rate of power loss at each step is obtained by the slope of the linear regression line through the power curves in Fig. 5. These degradation rates (absolute and relative) are summarized in Table 1 along with rates obtained from the constant current power densities in Fig. 4. With degradation rates on the order of a few mW cm^{-2} h^{-1}, the SOFC will not be able to sustain reasonable power generation for tens of thousands of hours, the current goal in SOFC technology.

A picture of the anode after removal from the furnace is shown in Fig. 1c. The outer rim of the anode is the characteristic dull grey of a Ni/YSZ anode after reduction of nickel oxide. The center of the anode is a shiny deposit that forms during exposure to PH_3. Evidence for the presence of nickel phosphides in this layer is given below.

An SEM image of the cross-section of the whole cell interface at lower magnification level is shown in Fig. 6a. The cathode layer is on top, the electrolyte layer is a thin light streak between anode and cathode, and the anode physical support layer (800 μm) is on the bottom. A closer examination of Fig. 6a and b reveals new layer (~20 μm thick) at the external surface of the anode. Two anode surface images, one from a protected part of the anode (Fig. 6c) and the other from the anode surface exposed to PH_3 (Fig. 6d), are compared at the same magnification. The protected anode surface has many submicron pores. The exposed anode surface shows the presence of a highly crystalline layer with considerably fewer pores, each pore larger than 1 micron. Comparison of these two anode surfaces also supports the nickel migration processes during PH_3 exposure.

The X-ray diffraction spectrum of the Ni–YSZ anode surface (Fig. 7) after exposure to PH_3 shows the presence of YSZ, Ni_3P, and Ni phases. The five peaks at 30.12°, 34.91°, 50.19°, 59.65° and 62.60° are assigned to YSZ (PDF #: 01-082-1241) by comparing the peak positions with literature values [14]. Ni_5P_2, Ni_3P, $Ni8P_3$ and $Ni_{12}P_5$ peaks may not be distinguished in XRD spectra due to the very close diffraction values of these chemical structures. However, the 36.38°, 41.77°, 42.82°, 43.67°, 45.29°, 45.08°, 46.65°, 52.77°, and 55.39° peaks are assigned to Ni_3P (PDF #: 34-501) by the software (X'Pert Highscore Plus) employed with the XRD instrument used in this study. The Ni_3P phase has been reported by Marina et al. [6,7] under these conditions. Trembly [15] and Xu et al. [4] reported that Ni_5P_2 is the main product with respect to thermodynamic equilibrium calculations for the contamination concentration of 2 and 10 ppm PH_3 in syngas. Metallic Ni (PDF #: 4-850) peaks appear at 44.51° and 51.85° but there are no peaks observed for NiO.

An XPS survey scan of the shiny metallic anode region seen in Fig. 1 is shown in Fig. 8. The Y and Zr peaks are not observed, which indicates that this metallic layer completely covers the Ni/YSZ composite. A similar survey scan on the anode surface underneath the mica gasket shows strong Y and Zr peaks and no P peaks (see Ref. [5] for an equivalent XPS survey scan). These observations support the Ni migration mechanism [5]. The detailed Ni 2p3 region scan is shown in the left inset of Fig. 8. The peak at 852.6 eV can be assigned to metallic nickel [16,17] and also to Ni–P alloys [18]. The P 2p binding energy region scan (right inset) shows two different P 2p peaks at 130.1 and 134.1 eV. These phosphorus peaks can be assigned to phosphorus with either a zero or negative oxidation state (130 eV) [19,20] and with a +5 oxidation state (134 eV) [20], respectively. The XPS data support the presence of a Ni_3P phase with possibly some metallic nickel. The 134 eV peak is tentatively assigned to phosphate formed on the surface of nickel phosphide during exposure to air.

The 20 μm spot XPS analysis is given in Fig. 9 as a scan on the cross-section of the anode active region next to the electrolyte. Peaks indicate the presence of C, O, Ni, Y, Zr, Si and P. Ni and P scans are shown in the insets of Fig. 9. The peak at 134 eV is assigned to phosphate in the active layer [2,18–20]. There is no visible evidence for phosphides (e.g., Ni_3P) in the active layer. However, a longer scan may be needed to detect other kinds of phosphorus compounds.

Table 1
Summary of degradation rates during and after the exposure to syngas with PH_3.

	Power density loss rate at constant voltage (mW cm^{-2} h^{-1})	Percent power loss rate (% h^{-1})	Power density loss rate at constant 1A current (mW cm^{-2} h^{-1})
PH_3 at 0.1 V	1.4	0.63	0.63
PH_3 at 0.2 V	0.4	0.13	0
PH_3 at 0.3 V	3.4	0.73	0.63
PH_3 at 0.1 V	0.33	0.21	0.84
PH_3 at 0.2 V	0.95	0.38	0.21
PH_3 at 0.3 V	0.98	0.30	1.6
Clean syngas at 0.2 V	0.10	0.03	−0.21
H_2 at 0.2 V	0.48	0.15	0.63

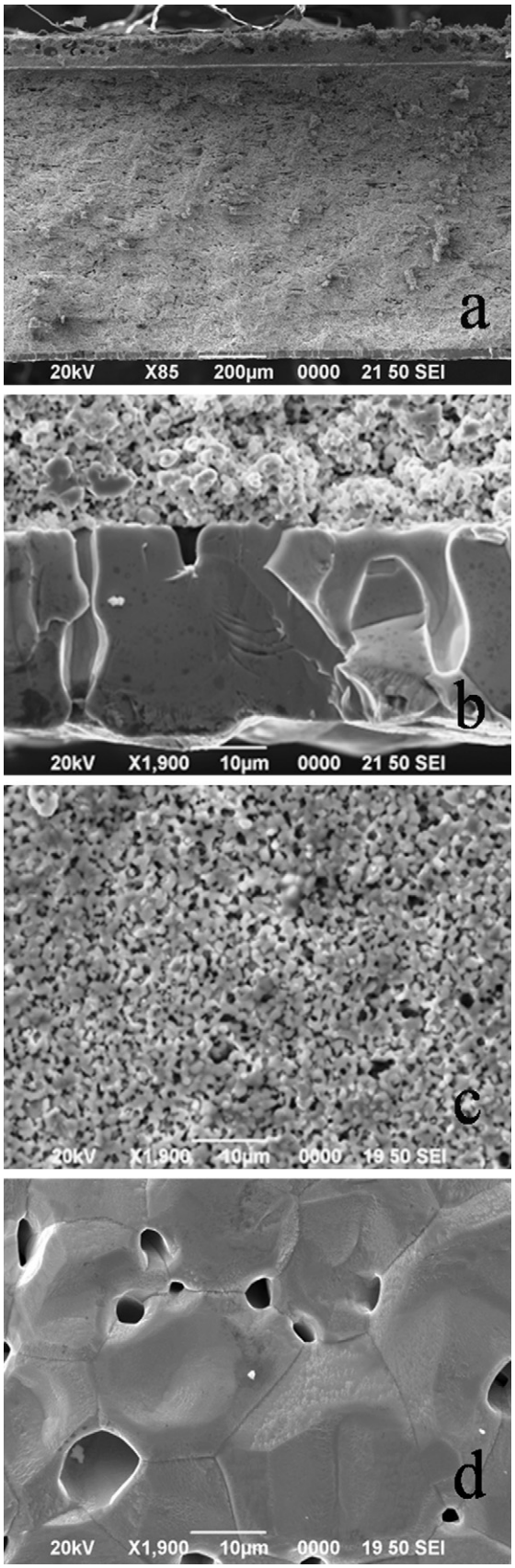

Fig. 6. SEM images of (a) the whole cell cross-section; (b) the cross-section of the shiny active anode surface; (c) the grey anode surface under the mica gasket; (d) the shiny active anode surface.

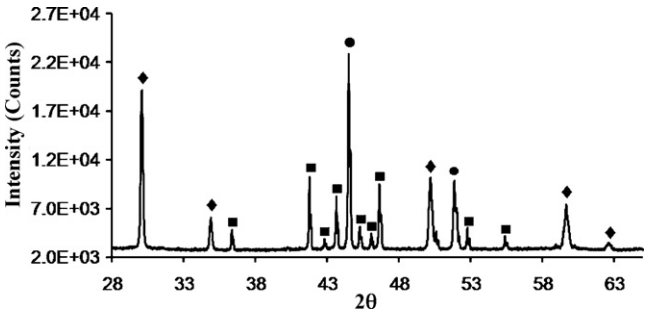

Fig. 7. XRD analysis of the Ni–YSZ anode-supported cell surface after 170 h of syngas with 10 ppm PH_3 exposure (♦: YSZ; ■: Ni_3P; and ●: Ni).

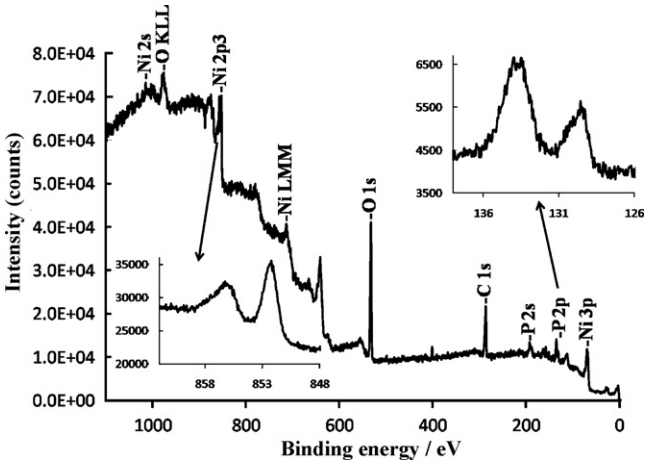

Fig. 8. XPS survey spectrum on shiny grey area. Inset: on the left is a detail scan over the Ni 2p3 range and on the right is a detail scan over the P 2p range.

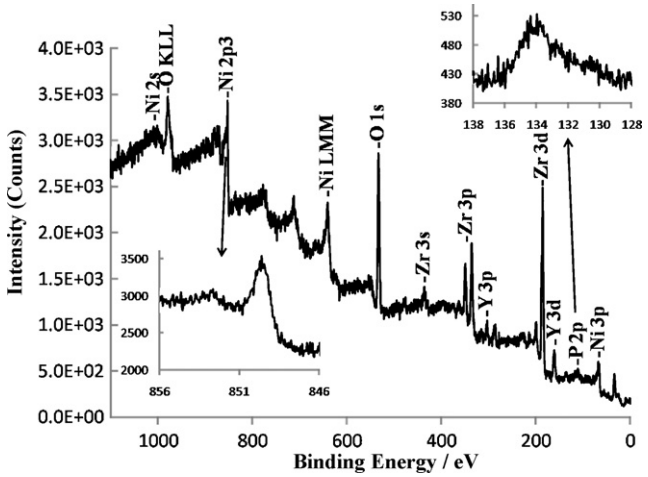

Fig. 9. XPS survey spectrum on the cross-section of the cell near to the active anode layer; inset: left is the detail scan over the Ni 2p3 range and right is the detail scan over the P 2p range.

4. Conclusion

Phosphorus poisoning of the Ni/YSZ anode has been investigated under both potentiostatic and galvanostatic conditions. The degradation begins as soon as PH_3 is added to the fuel stream and continues at all three overpotentials. There is no correlation between the overpotential and the power loss rate. The highest degradation rate is observed during the initial application of 0.3 V overpotential. Degradation continues for at least 24 h after PH_3 is

removed from the fuel stream, but that observation may be due to residual PH_3 in the gas transfer lines. The series and polarization resistances both increase during the initial exposure to PH_3, and the polarization resistance continues to increase after removal of PH_3. Post-mortem XRD analysis confirms the presence of nickel phosphide (especially Ni_3P) phases. SEM images show a new layer formed on the external surface of the anode. Nickel migrates through the anode structure to the anode surface to form a new layer of nickel and/or nickel phosphide.

Acknowledgements

This project is sponsored by US DOE-EPSCoR Program. NETL (National Energy Technology Laboratory), US DOE Office of Basic Energy Sciences, WV State EPSCoR Office and West Virginia University provide the support to this study under the grant number of DE-FG02-06ER46299. In this project the DOE Technical Monitor is Dr. Tim Fitzsimmons, the Administrative Manager is Dr. Richard A. Bajura and the Technical Manager and Principal Investigator is Dr. Ismail Celik. The authors would like to express gratitude to Dr. Andy Woodworth for XPS data, Dr. Keith Morris for SEM data and Dr. Yun Chen for XRD data.

References

[1] F.N. Cayan, M.J. Zhi, S.R. Pakalapati, I. Celik, N.Q. Wu, R. Gemmen, J. Power Sources 185 (2008) 595–602.
[2] M.J. Zhi, X.Q. Chen, H. Finklea, I. Celik, N.Q. Wu, J. Power Sources 183 (2008) 485–490.
[3] J. Bao, G.N. Krishnan, P. Jayaweera, J. Perez-Mariano, A. Sanjurjo, J. Power Sources 193 (2009) 607–616.
[4] C.C. Xu, J.W. Zondlo, H.O. Finklea, O. Demircan, M.Y. Gong, X.B. Liu, J. Power Sources 193 (2009) 739–746.
[5] O. Demircan, C.C. Xu, J. Zondlo, H.O. Finklea, J. Power Sources 194 (2009) 214–219.
[6] O.A. Marina, L.R. Pederson, D.J. Edwards, C.A. Coyle, J. Templeton, M. Engelhard, Z. Zhu, Proceedings of the 8th Annual SECA Workshop, San Antonio, TX, 2007.
[7] O.A. Marina, L.R. Pederson, C.A. Coyle, E.C. Thomsen, D.J. Edwards, G.W. Coffey, C.N. Cramer, B.W. Arey, Y.S. Chou, Proceedings of the 10th Annual SECA Workshop, Pittsburgh, PA, 2009.
[8] H. Kishimoto, K. Yamaji, M.E. Brito, T. Horita, H. Yokokawa, J. Mining Metall. B Metall. 44 (2008) 39–48.
[9] S.W. Zha, Z. Cheng, M.L. Liu, J. Electrochem. Soc. 154 (2007) B201–B206.
[10] Z. Cheng, S.W. Zha, M.L. Liu, J. Power Sources 172 (2007) 688–693.
[11] A. Bieberle, L.P. Meier, L.J. Gauckler, J. Electrochem. Soc. 148 (2001) A646–A656.
[12] S.P. Jiang, Y. Ramprakash, Solid State Ionics 122 (1999) 211–222.
[13] W.G. Bessler, J. Warnatz, D.G. Goodwin, Solid State Ionics 177 (2007) 3371–3383.
[14] M.B. Pomfret, C. Stoltz, B. Varughese, R.A. Walker, Anal. Chem. 77 (2005) 1791–1795.
[15] J.P. Trembly, Investigation into the effects of trace coal syngas species on the performance of solid oxide fuel cell anodes, Ph.D. Dissertation, Ohio University (2007).
[16] J.F. Moulder, W.F. Stickle, P.E. Sobol, K.D. Bomben, Handbook of X-ray Photoelectron Spectroscopy, Physical Electronics, Eden Prairie, MN, 1995.
[17] A.B. Mandale, S. Badrinarayanan, S.K. Date, A.P.B. Sinha, J. Electron Spectrosc. Relat. Phenom. 33 (1984) 61–72.
[18] M.G. Thube, S.K. Kulkarni, D. Huerta, A.S. Nigavekar, Phys. Rev. B 34 (1986) 6874–6879.
[19] B. Elsener, M. Crobu, M.A. Scorciapino, A. Rossi, J. Appl. Electrochem. (2008) 1053–1060.
[20] R. Franke, Spectrochim. Acta Pt. A Mol. Biomol. Spectrosc. 53 (1997) 933–941.